Chapter 4

Imaging complex structures with layer-stripping depth migration

In this chapter I describe how to combine Kirchhoff datuming with Kirchhoff migration to image complex structures with first-arrival traveltimes from a finite-difference solution to the eikonal equation. The novel concept presented in this chapter is that by breaking up a complex velocity model, it is possible to calculate traveltime tables for migration that are well behaved and that produce excellent images.

The hybrid layer-stripping migration algorithm produces accurate images of complex structures by downward continuing the data and imaging from a lower datum. The method alternates steps of datuming and imaging. Because traveltimes are computed for each step, the adverse effects of caustics, headwaves, and multiple arrivals do not develop. In principle, this method only requires the same number of traveltime calculations as a standard migration.

Using the Marmousi synthetic data set, I compare the result of the layer-stripping migration to images obtained with standard migration algorithms and also with Kirchhoff migration using traveltimes from maximum-amplitude paraxial ray tracing and a band-limited Green's function method.

4.1 Kirchhoff imaging of complex structures

Kirchhoff migration is generally accepted to be the most efficient method of imaging 2-D and 3-D prestack seismic data. However, many researchers have discovered that

Kirchhoff algorithms that use first-arrival traveltimes do a poor job of imaging complex structures. (Audebert et al., 1994b; Gray and May, 1993; Geoltrain and Brac, 1993). Even methods which calculate multiple arrivals and most energetic arrivals along with estimates of amplitude and phase do not always result in satisfactory images. It is generally accepted that algorithms which use recursive wavefield continuation to backwards propagate the received wavefield produce the best images. Unfortunately, these methods often require regular spatial sampling and are computationally intensive. That is why nonrecursive methods based on the Kirchhoff integral are attractive, especially for 3-D prestack imaging objectives. Kirchhoff algorithms can easily accommodate irregular sampling and they can be applied in a target-oriented fashion. The use of first-arrival traveltimes is popular because they are efficiently computed and they have the attractive property of filling the entire computational grid.

In their 1993 *Geophysics* article, Geoltrain and Brac ask the question "Can we image complex structures with first-arrival traveltime?" They conclude that they cannot, and that they should either ray trace to find the most energetic arrivals, or calculate multiple-arrival Green's functions. Nichols (1994) calculates band-limited Green's functions to estimate the most energetic arrivals. He estimates not only traveltime, but also amplitude and phase. Both these approaches are computationally complex and much more costly than first-arrival traveltime computation methods. My approach is simpler: by breaking up the complex velocity structure, I am able to calculate traveltimes in velocity models where finite-differencing the eikonal equation is valid. This results in images comparable to those obtained by Nichols' method and by shot-profile migration at a reduced computational cost.

4.1.1 The Marmousi synthetic data set

The Marmousi synthetic data set (Bourgeois et al., 1991) was first released as a blind test for velocity estimation, but when the velocity model was revealed, it was discovered that many migration algorithms failed, so it has become a popular testbed for migration algorithms. It is a complex acoustic 2-D data set based on the geology of the Cuanza basin in Angola. The velocity model is shown in Figure 4.1. Its structural style is dominated by growth faults which arise from salt creep and give rise to the complicated velocity structure in the upper part of the model. The main imaging objective is the reservoir in the anticlinal structure below the salt.

The synthetic data set consists of 240 shots with 96 gathers each. The representative shot gathers in Figure 4.2 display complicated nonhyperbolic moveout, clearly indicating that this is a depth-imaging problem. Zero-phase source deconvolution was applied to the data used in this study as part of the preprocessing (Barut et al., 1991). The same four representative shot gathers are displayed after preprocessing in Figure 4.3.

4.2 First-arrival traveltimes in complex velocity models

Finite-difference solutions to the eikonal equation are attractive for generating traveltime tables for Kirchhoff migration because their implementations are generally fast and efficient. The traveltimes are smooth and they fill the computational grid. Throughout this study, I use an upwind finite-difference solution to the eikonal equation to generate traveltimes (van Trier and Symes, 1991; Popovici, 1991).

Green's functions based on first-arrival traveltime calculation methods result in poor images in structurally complex areas. Several reasons have been given for this failure:

- The high-frequency approximation of ray and eikonal methods breaks down in complex velocity models. In rapidly varying velocity models, different frequency components of the wavefield propagate at different velocities; therefore, summation trajectories based on only the high-frequency components may not capture the desired events.

- When high velocity zones are present, the first-arrivals may be non-energetic headwaves.

- As energy propagates in complex models, raypaths tend to cross eventually. This causes phase shifts and triplications. First-arrival traveltimes follow the fastest branch of the triplication bow-tie, which is also the low-energy branch.

Complexity of velocity models and validity of high-frequency approximations can be defined in various ways. In a large-scale depth model, there can be considerable relative changes in velocity. Changes in velocity distort the shape of the wave propagation front and create more opportunities for frequency components to separate, for headwaves to develop, and for triplications to occur. By dividing the depth model into small areas, I obtain a traveltime propagation front that better matches the wave equation propagation front. Therefore, imaging with first-arrival traveltimes is more accurate.

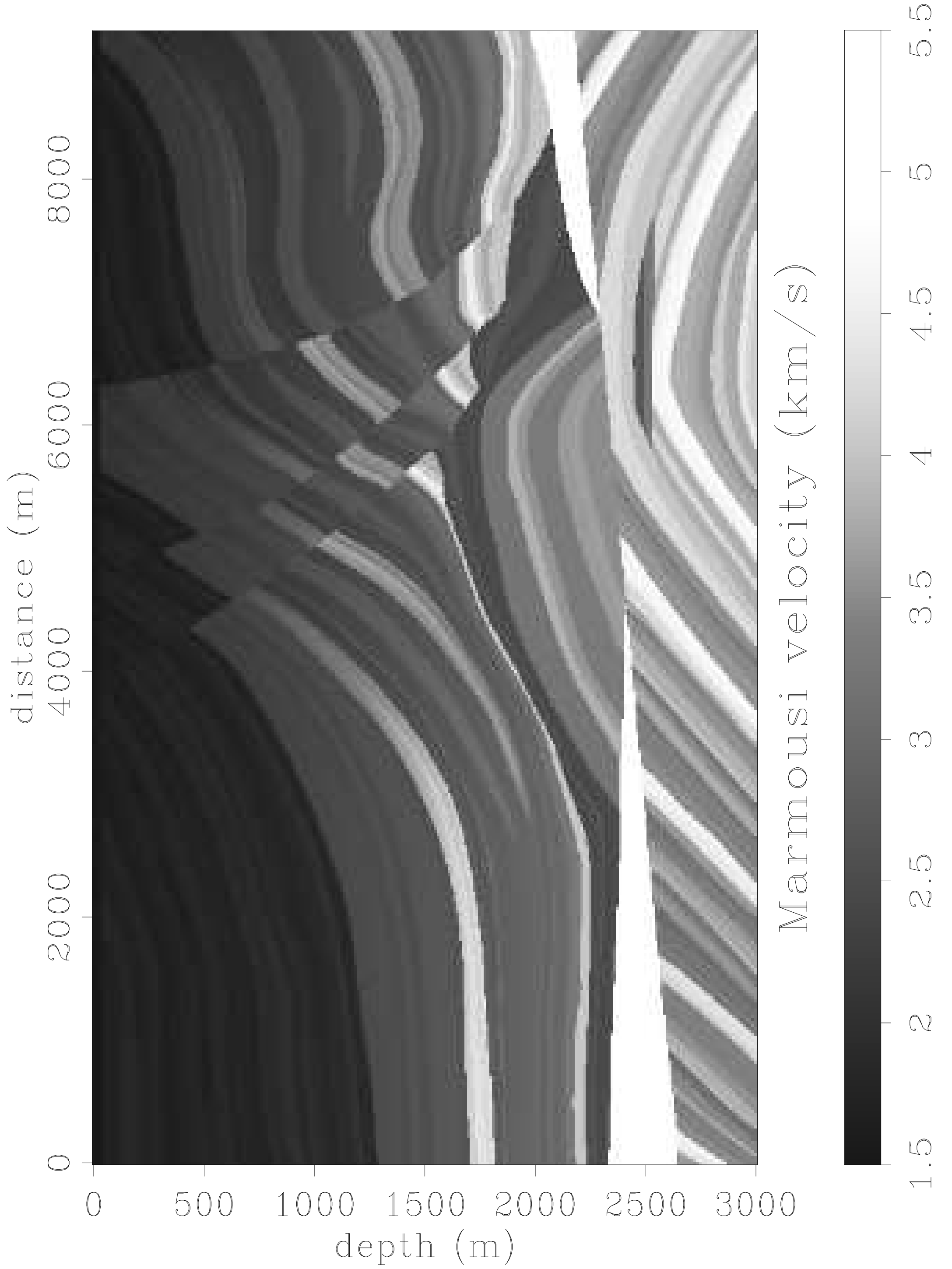

FIG. 4.1. The Marmousi velocity model. Layer-velfig [R]

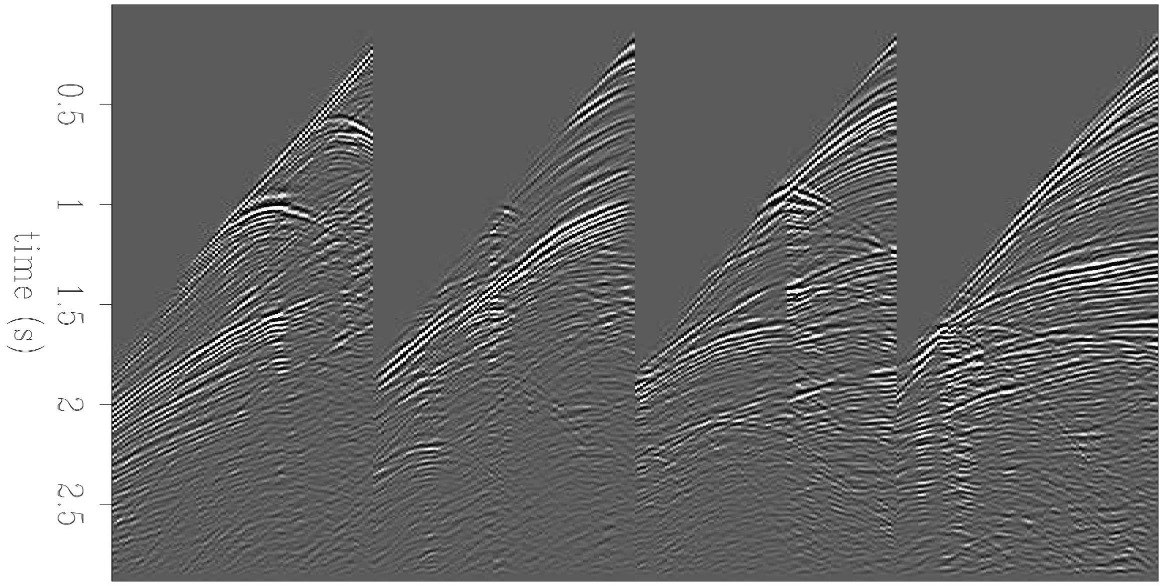

FIG. 4.2. Some representative shot gathers from the Marmousi synthetic data set. Layer-marmshts [R]

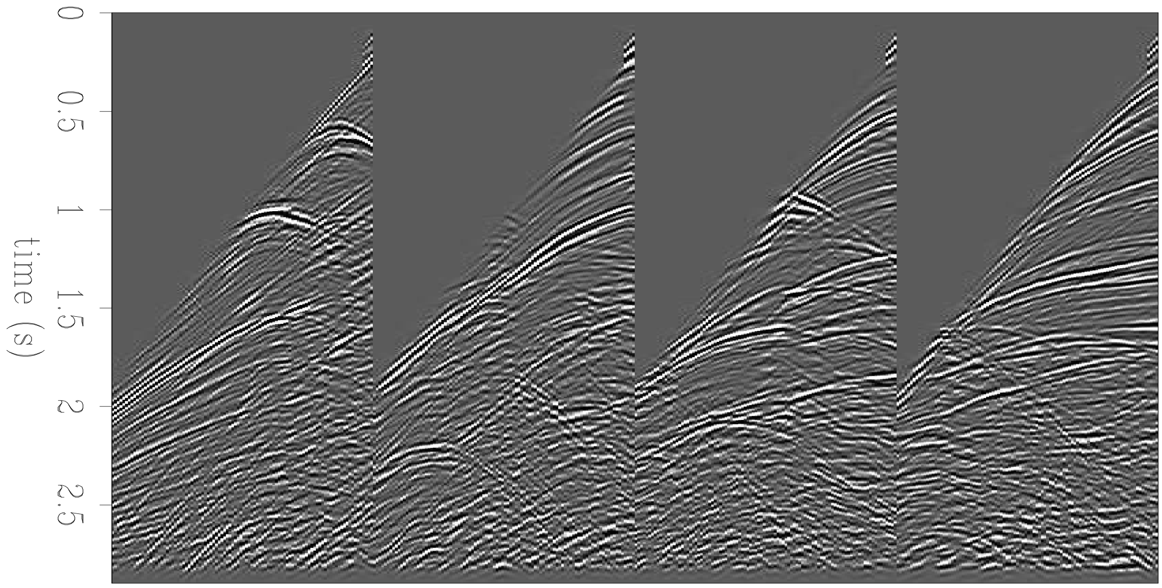

FIG. 4.3. Representative shot gathers from the Marmousi synthetic data set after preprocessing. Movie. Layer-preshts [R]

4.2.1 Comparison of acoustic wavefields and first-arrival traveltimes

The Marmousi velocity model (Figure 4.1) generates complex propagation paths in which late energetic arrivals are not fit well by first-arrival finite-difference traveltimes. In Figures 4.4 through 4.6, a modeling program written by Martin Karrenbach (1995) is used to generate snapshots of the acoustic wavefield from two surface locations in the Marmousi model. The corresponding contours of first-arrival traveltime have been overlaid. These contours are from the first-arrival traveltime tables used for Kirchhoff datuming and migration later in this chapter.

At the early-time snapshots displayed in Figure 4.4, the first-arrival contours overlay the energetic portions of the wavefield nicely. This is because there has not been enough time for adverse propagation effects to develop fully. Since the first-arrival traveltime matches the high energy portions of the wavefield, using these traveltimes for Kirchhoff migration will result in good imaging at these early times.

In contrast, snapshots for the same source locations at later times of 0.9 s and 1.05 s (Figure 4.5) show that the first-arrival traveltimes do not always correspond to energetic portions of the wavefield. If these traveltimes were used for migration, the resulting image would suffer because parts of the summation trajectories would not correspond to energetic arrivals. This last sequence of two figures demonstrates that as the wavefield evolves, complex propagation effects begin to manifest themselves, and the first-arrival traveltimes no longer match the most energetic wavefront.

Figure 4.6 is generated by starting the acoustic modeling and the first-arrival traveltime calculation from a depth of 1500 m. The 0.2 s and 0.3 s contours correspond nicely to the high energy portions of the wavefields. There is some deviation in the shallow part of the lower left 0.3 s panel, but for the most part, the first-arrival traveltime contour fits the bulk of the acoustic energy very well. The pulling away of the first-arrival traveltime contour represents a headwave propagating along the thin high velocity layer that starts under the fault at lateral position of about 5500 m and a depth of 1500 m in Figure 4.1.

Overall, the contours in Figure 4.4 and 4.6 have not pulled away from the energetic wavefront as they have in Figure 4.5. This shows that if traveltime calculation is limited to early times, the first-arrival traveltimes accurately parameterize the most energetic portions of the acoustic wavefield.

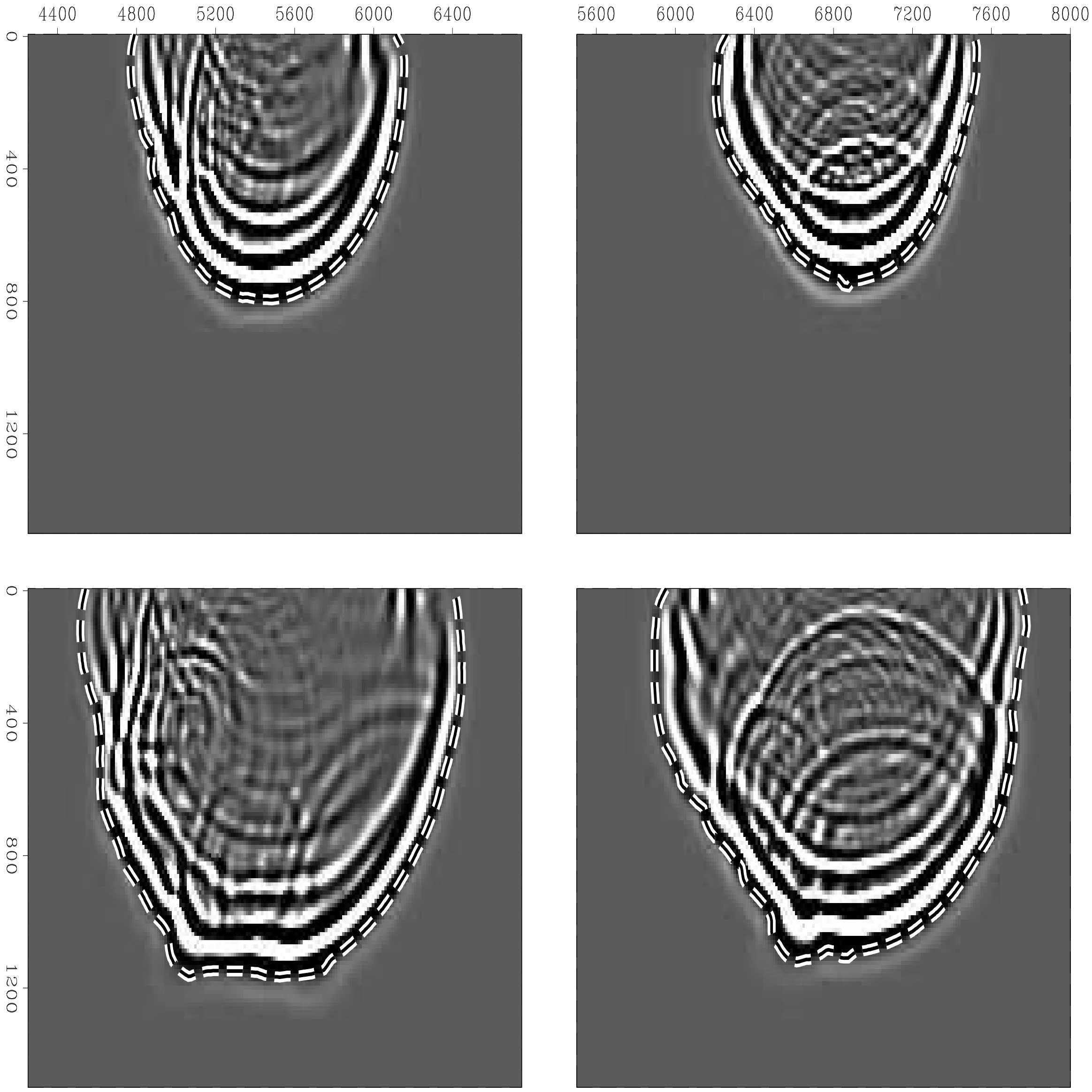

FIG. 4.4. Acoustic wavefield modeling overlaid by contours of first-arrival traveltime. The top snapshots are at 0.4 s, the bottom two are at 0.55 s for surface source locations at 5425 m and 6887.5 m in the Marmousi model. Movie. Layer-snapearly [CR]

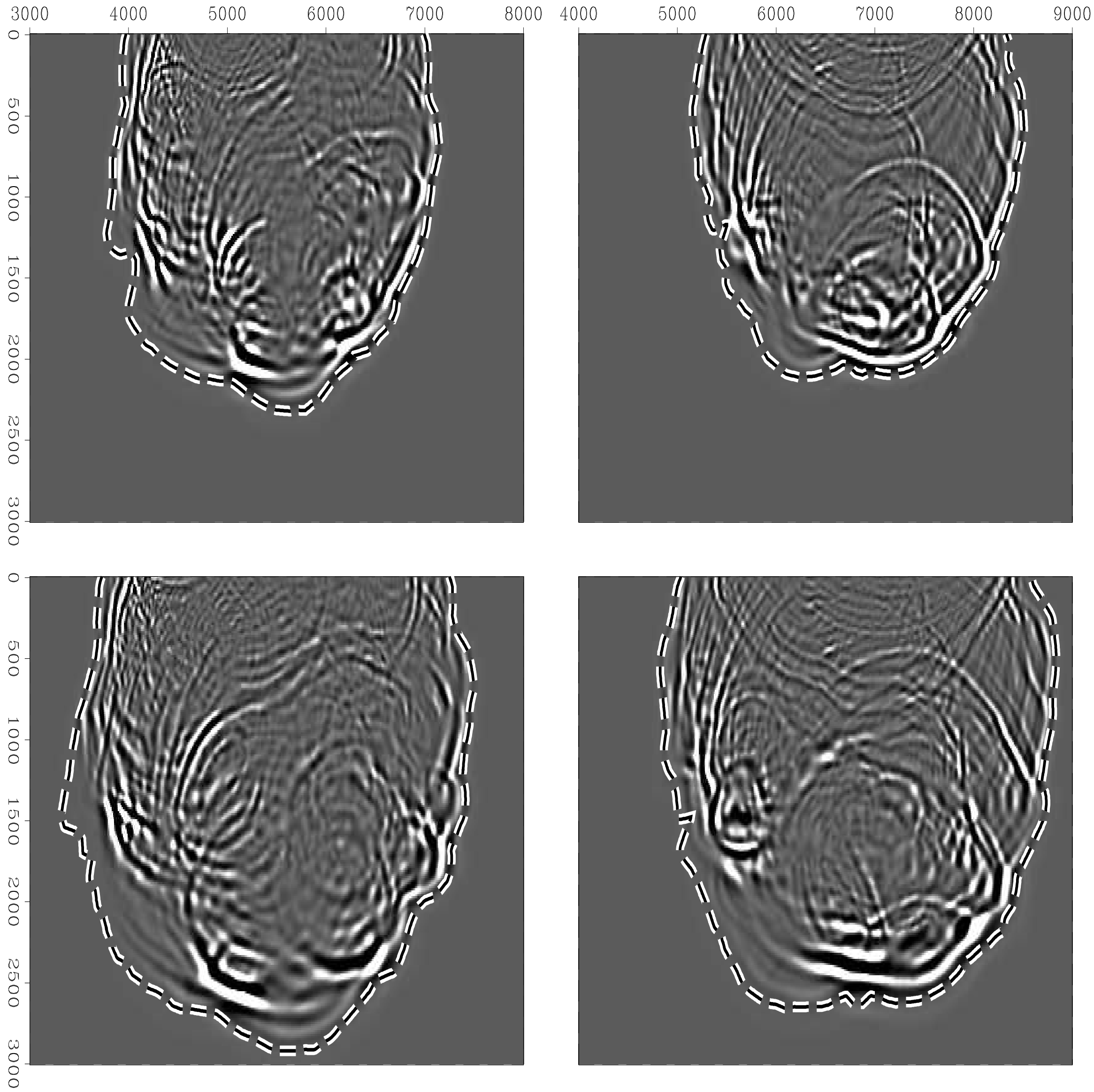

FIG. 4.5. Acoustic wavefield modeling overlaid by contours of first-arrival traveltime. The top snapshots are at 0.9 s, the bottom two are at 1.05 s for surface source locations at 5425 m and 6887.5 m in the Marmousi model. Movie. Layer-snaplate [CR]

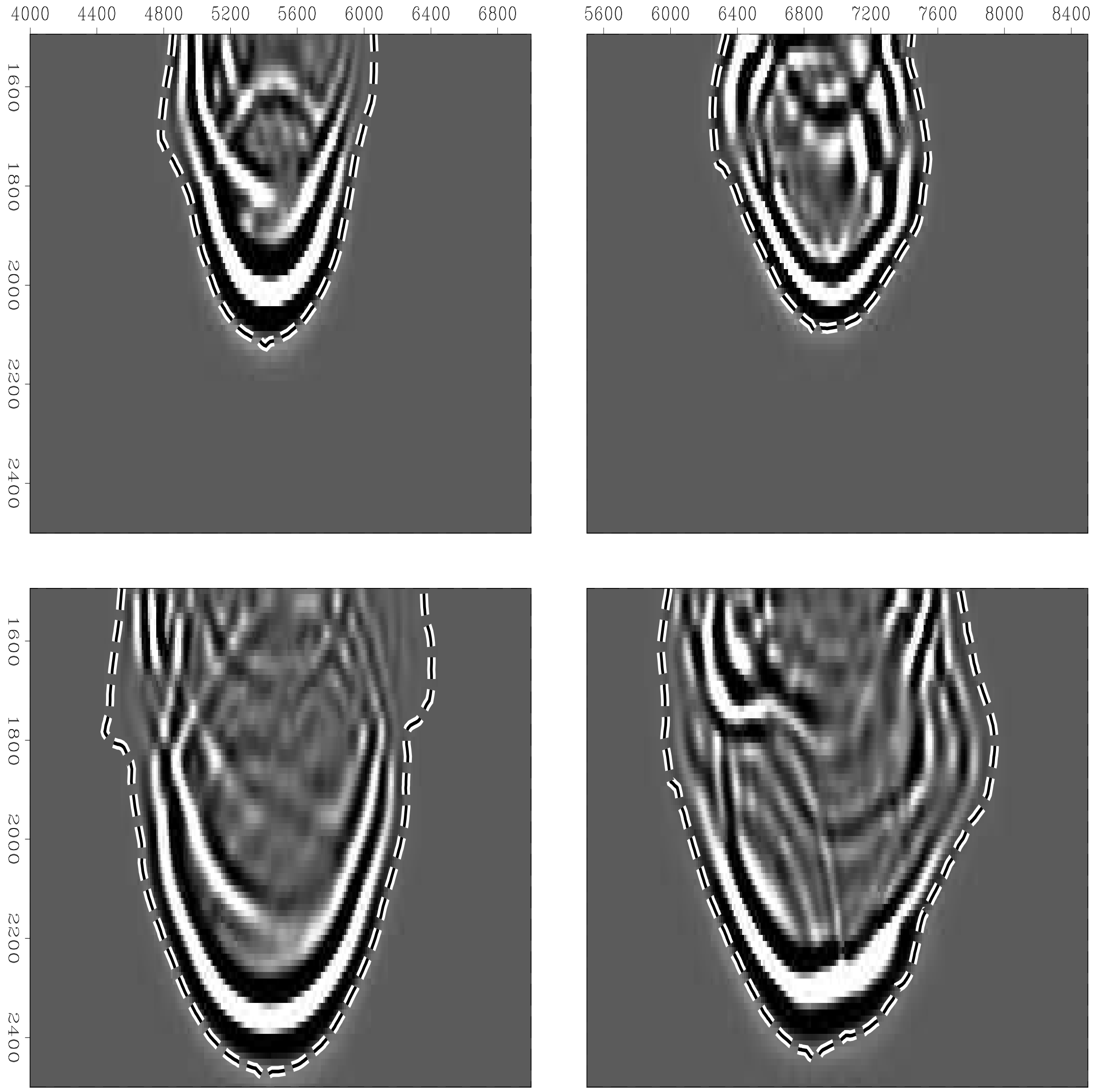

FIG. 4.6. Acoustic wavefield modeling overlaid by contours of first-arrival traveltime. Snapshots are taken at the same two lateral locations as in Figures 4.4 and 4.5 but with sources at a depth of 1500 m. The top two panels are at a time of 0.2 s and the bottom two are at a time of of 0.3 s. Layer-snapdatum [CR]

4.2.2 Imaging with first-arrival traveltimes

Figure 4.7 is the result of an industry standard Kirchhoff migration of the Marmousi synthetic using first-arrival traveltimes calculated with a finite-difference eikonal equation solver. The faults and beds in the upper portion are well imaged; however, the anticlinal structure below 2300 m and the target zone at a lateral position of about 6500 m and depth of 2500 m is not imaged.

The migration result corresponds exactly to the observations made in comparing the acoustic wavefield modeling to contours of first-arrival traveltime. The upper 1500 m to 2000 m of the migration which is well imaged corresponds to the wavefields and contours of Figure 4.4. In this part of the model, the first-arrival traveltimes accurately parameterize the high energy portion of the wavefield. The left and right sides of the figure are nicely imaged because the velocity model is relatively simple in these areas. The central portion of the image, at the target zone, corresponds to the wavefields and traveltime contours of Figure 4.5. The propagation here is complicated by the overlying faults which contain fast and slow velocity regions, and by the high velocity salt which partially overlays the target.

The properties of first-arrival traveltimes described in the preceding section, as well as the observation that Kirchhoff migration using first-arrival traveltimes produces an acceptable image of the upper part of the Marmousi synthetic, motivated the development of the layer-stripping method described next.

4.3 Layer-Stripping Kirchhoff migration

The premise of the layer-stripping method is that data can be re-synthesized at any subsurface datum by downward continuation with the adjoint Kirchhoff datuming algorithm. The depth step of the datuming is limited so that the first-arrival traveltimes are calculated in such a way that they accurately parameterize the most energetic portions of the wavefield. In this way, the downward continued data are accurately synthesized at a datum which is closer to the imaging target. Traveltimes can then be calculated from the new datum, and the data can either be downward continued again or migrated from the new datum.

Since all the traveltimes in this process are calculated over a smaller portion of the velocity model, the final outcome is a more accurate image.

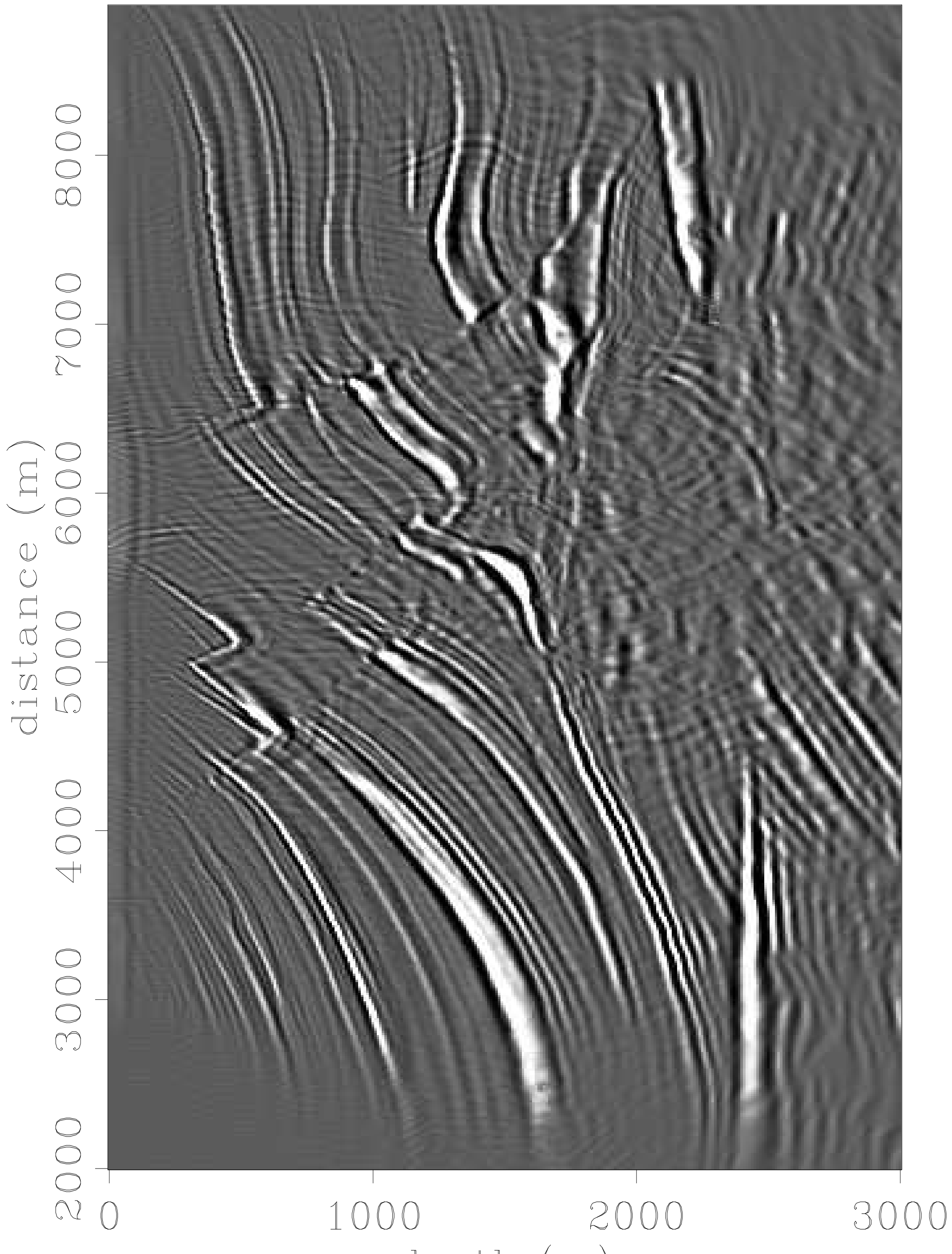

FIG. 4.7. Standard Kirchhoff migration using first-arrival traveltimes. Movie. Layer-standard [CR]

4.3.1 Layer-stripping Kirchhoff as a semi-recursive method

The layer-stripping migration method can be thought of as a hybrid algorithm that incorporates some of the advantages of recursive migration with the efficiency of Kirchhoff migration. I call it semi-recursive because the depth step is much greater than that used in phase-shift or finite-difference shot-profile migrations. Because the data are re-synthesized at one or more depth levels in the subsurface, the method has the added advantage of implicitly handling multiple arrivals. In each datuming and imaging step the traveltime tables are single valued, but because the data are repropagated at every step, the final effect is equivalent to using multivalued traveltime tables.

This is illustrated by Figures 4.8 through 4.10, which compare recursive migration to standard Kirchhoff migration, and to the layer-stripping method. In a recursive method such as shot-profile migration, shots and geophones are downward continued through each depth level. Figure 4.8 illustrates this for one line of shots or geophones. It is evident that there are many propagation paths from the surface to the image point; therefore, multiple arrivals are handled. The computation is performed for all frequencies.

By contrast, first-arrival Kirchhoff migration is performed by summing data over trajectories defined by the propagation paths illustrated in Figure 4.9. There is only one path linking each surface position to the image point; therefore, multiple arrivals are not handled. Although crossing paths are not illustrated here, they can occur.

The layer-stripping method is illustrated in Figure 4.10. It is a combination of Kirchhoff wave-equation datuming and Kirchhoff migration. There are multiple propagation paths from the surface to the image point; therefore, multiple arrivals are handled. The computation is illustrated for the Marmousi model in Figure 4.11 and proceeds as follows:

1. Calculation of traveltimes from the surface (Figure 4.11a). These traveltimes are used to:
   - Migrate from the surface to some depth level z_1 or lower.
   - Downward continue to depth level z_1 (Figure 4.11b).
2. Calculation of traveltimes from depth level z_1 (Figure 4.11c). These traveltimes are used to:
   - Migrate from depth level z_1 (Figure 4.11d).

The depth step of Kirchhoff downward continuation is much larger than the $\triangle z$ used in shot-profile migration. Since there are multiple paths from the surface to the image point, multiple arrivals are handled. Because the paths are shorter than in Figure 4.9, first-arrival traveltimes are more likely to be valid.

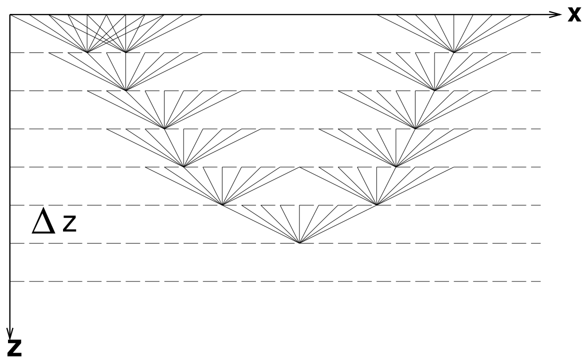

FIG. 4.8. A few representative propagation paths from the surface to an image point for shot-profile migration. There are many paths from each surface location to the depth point. Layer-s-g [NR]

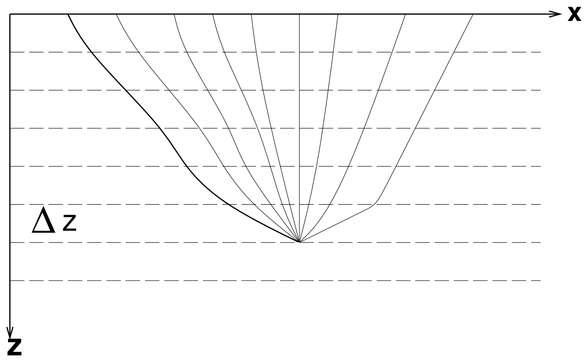

FIG. 4.9. Propagation paths from the surface to an image point for Kirchhoff migration. There is only one path from each surface location to the depth point. Layer-kirch [NR]

4.3.2 Marmousi example

The last image of Figure 4.11 is displayed at full scale in Figure 4.12. It is generated by downward continuing the data to a depth of 1500 m in one datuming step. The downward continued data are then migrated and combined with the previous image of the upper 2000 m. This overlap is used to preserve image quality because the portion of the image directly below the 1500 m datum suffers from the effects of limited offset and near-field Kirchhoff distortion. The overlap simply avoids the near-surface distortion suffered by

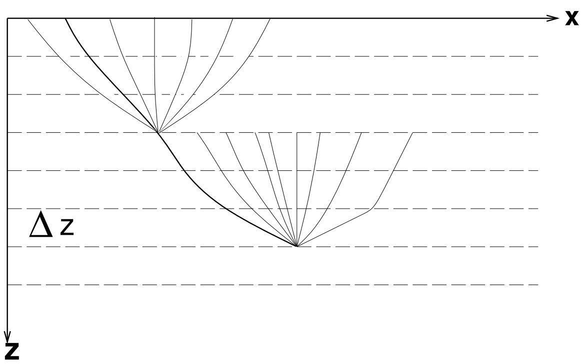

FIG. 4.10. Propagation paths from the surface to a depth point for layer-stripping Kirchhoff downward continuation and migration. Paths traverse shorter distances so they are less likely to cross, and there are multiple paths to each depth point. Layer-datum [NR]

most Kirchhoff migration algorithms.

Figure 4.12 is a clear improvement over the standard migration displayed in Figure 4.7. The anticlinal structure below the salt and the target are now clearly imaged.

An even greater imaging improvement is attained by making the datuming step shorter since this insures that the first-arrival traveltimes are a better approximation to the most energetic arrivals. Continuation of the data to 1500 m in three steps of 500 m each, results in an even better-focused image of the anticline and the target (Figure 4.13). In both Figure 4.12 and 4.13, the events which unconformably define the top of the anticline, the anticline events themselves, and the target events are clearly imaged. The lateral continuity and event coherency in the target zone are substantially improved in Figure 4.13.

In Figure 4.14, I compare the images in the vicinity of the target zone to the velocity model and a synthetic reflectivity model which represents the desired image. The synthetic reflectivity (Figure 4.14b) is obtained by combining the velocity and density models and convolving with a wavelet. This type of resolution cannot be expected from migration, but ideally, the migration results should provide a comparable structural image.

Both of the layer-stripping images in Figures 4.14c and 4.14d compare favorably with the desired reflectivity. The image obtained by downward continuing the data in three steps of 500 m is superior since the events display better lateral continuity and the image is clearer. This is because the traveltimes calculated for each of the 500 m steps are better behaved than the traveltimes calculated for one step of 1500 m. The resolution is so good that the flat spot in the reservoir and the strongly reflective cap stand out clearly. The phase of the events is a good match to that of the synthetic reflectivity section.

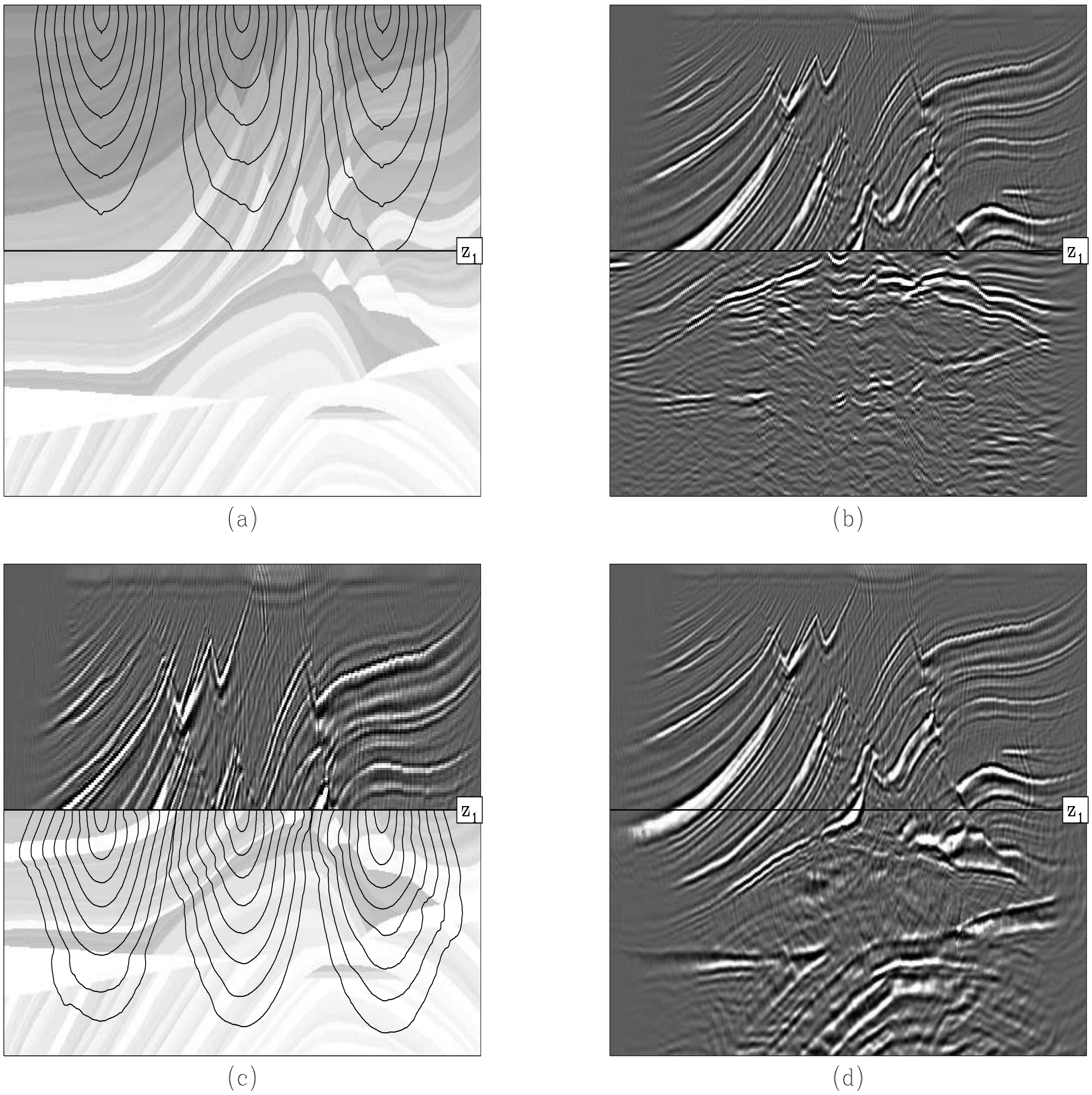

FIG. 4.11. Illustration of layer-stripping Kirchhoff datuming and migration. The velocity model is divided into two parts. (a) Finite-difference traveltimes are calculated in the upper part of the model. (b) These traveltimes are used to image the upper portion of the data and downward continue the wavefield, resynthesizing it at depth level z_1. (c) Traveltimes are calculated from depth level z_1 and (d) used to image the downward continued wavefield. Movie. $\boxed{\text{Layer-calc}}$ [CR]

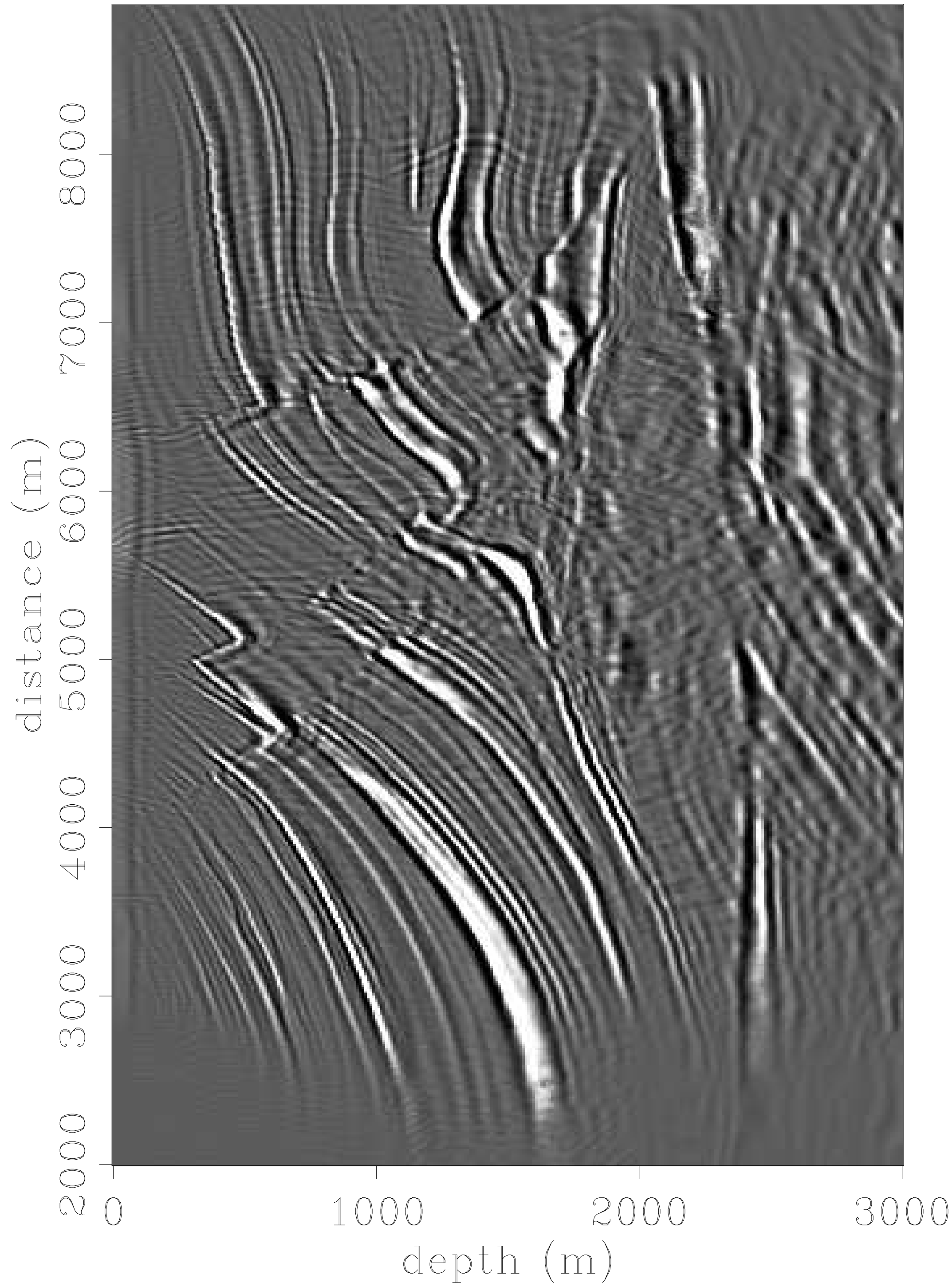

FIG. 4.12. Migrated image using traveltimes calculated from the surface, and traveltimes calculated from a depth of 1500 m. The lower part of the image was obtained by migrating data which was redatumed to a depth of 1500 m in one step of downward continuation. Movie. Layer-strip1 [CR]

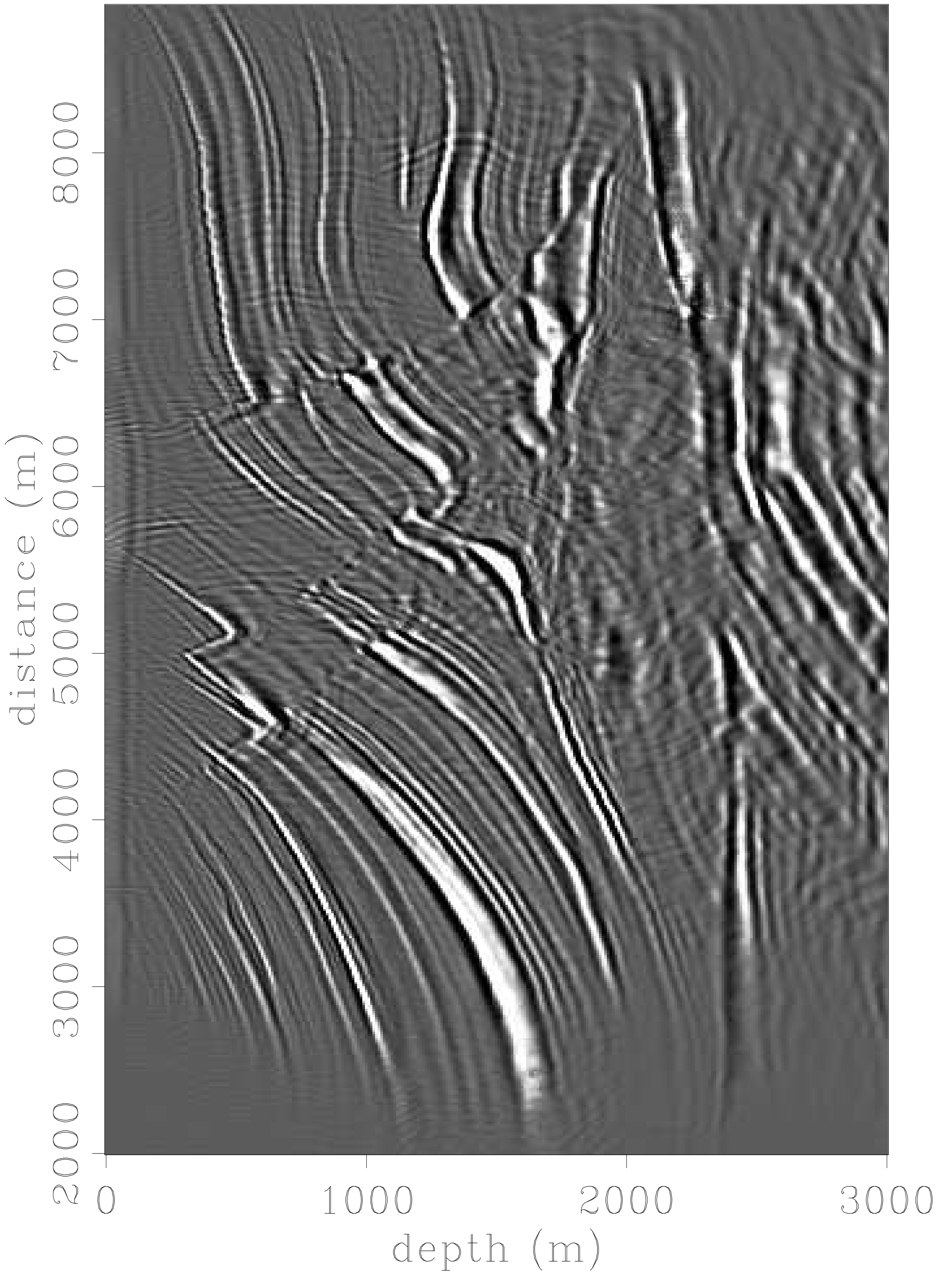

FIG. 4.13. Migrated image using traveltimes calculated from the surface, and traveltimes calculated from a depth of 1500 m. The lower part of the image was obtained by migrating data which was redatumed to a depth of 1500 m in three steps of 500 m each. Movie. Layer-strip3 [CR]

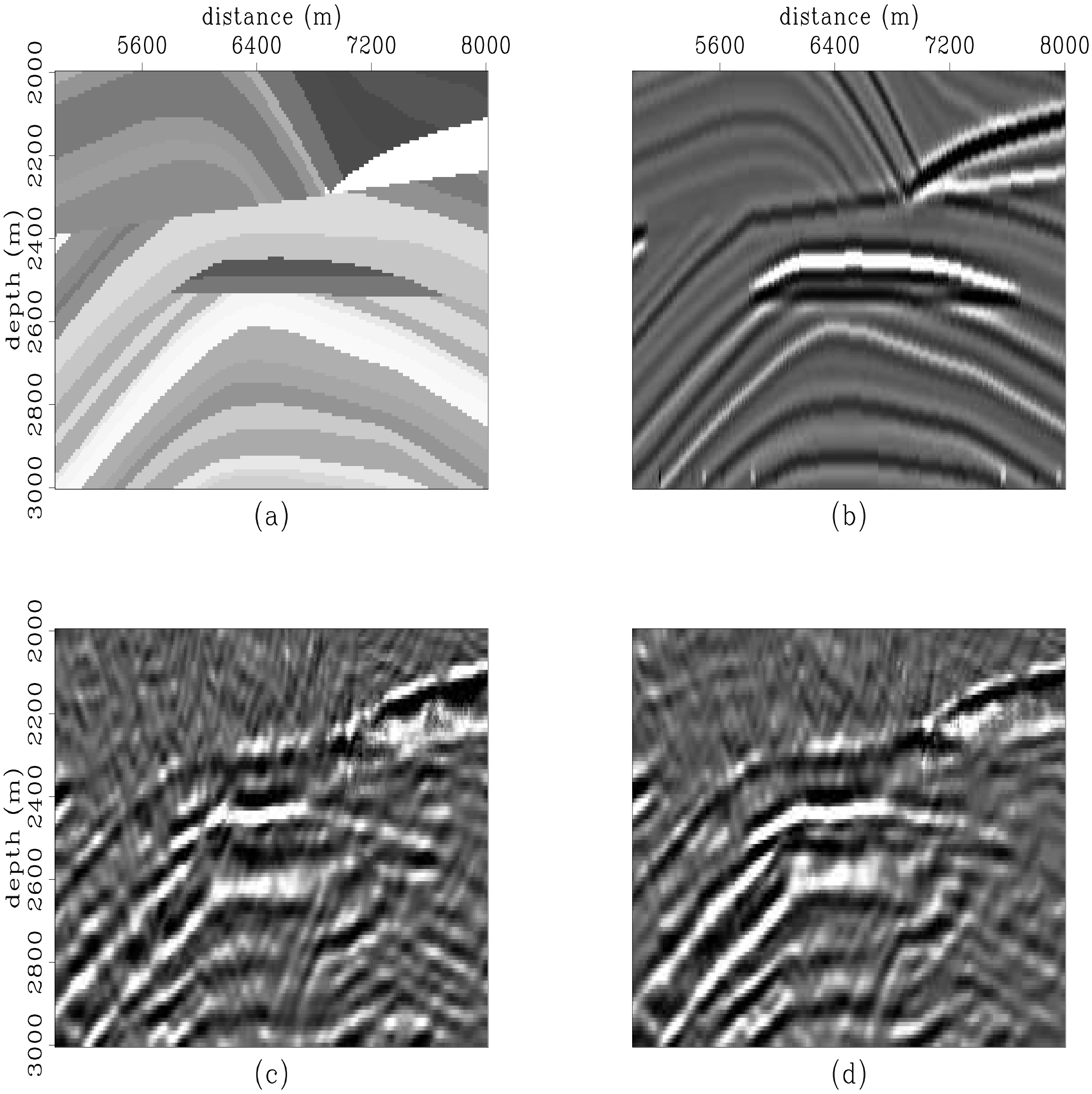

FIG. 4.14. Closeup comparison at the target zone of (a) the velocity, (b) the ideal reflectivity, (c) the image after downward continuation to 1500 m in one step, and (d) the image after downward continuation to 1500 m in three steps of 500 m each. Movie. $\boxed{\text{Layer-targref}}$ [CR]

4.4 Comparison to other migrations

In this section I compare my layer-stripping migration algorithm to shot-profile migration, and Kirchhoff migration using both maximum-amplitude traveltimes and band-limited Green's functions.

The shot-profile migration generated with Advance Geophysical Co.'s commercial algorithm is displayed in Figure 4.15. It produces a good structural image by recursively downward continuing source and receiver wavefields for all frequencies using explicit finite-difference extrapolators. The problem with the method is that it is expensive and it requires regular fine sampling of the recording surface. This makes it impractical for 3-D data and irregularly-sampled land data.

Figure 4.16 is the result of Kirchhoff migration using maximum-amplitude traveltime and phase calculated with a paraxial ray-tracing program. Thorbjorn Rekdal did the ray tracing and Dave Nichols did the migration to produce this image (Nichols, 1994). This results in a much better image than the standard first-arrival traveltime migration of Figure 4.7, but it is not as good as my layer-stripping Kirchhoff migration. It shows that there is an advantage to maximum-amplitude ray tracing, but that the complexity of the wavefield cannot be adequately accounted for at late times. This method is generally pretty expensive and requires extensive smoothing of the slowness model to ensure stability of ray tracing.

Figure 4.17 is the result of using Nichols' (1994) band-limited Green's function method to calculate traveltimes for Kirchhoff migration. The image is much better than the standard first-arrival traveltime migration of Figure 4.7, but, once again, it is not as good as my layer-stripping Kirchhoff migration. The figure shows that using traveltimes which are calculated in the seismic frequency band has a distinct advantage over first-arrival traveltimes and that the band-limited traveltimes track the high energy portions of the wavefield better, but they are still not able to capture all the events which should be summed coherently to form the best image. Nichols' method is considerably less expensive than shot-profile migration because only eight frequency components are propagated to estimate band-limited traveltimes; however, it is more expensive than finite-difference first-arrival traveltime calculation.

The target zone images of the Kirchhoff migration results are compared in Figure 4.18. The layer-stripping migration produces the best image. It is the best match to the idealized reflectivity, and it has the best overall image quality in terms of lateral continuity and structural definition.

4.5 Imaging with an approximate velocity model

All of the previous results were obtained using the exact Marmousi velocity model, but in a real exploration scenario the determined velocity model would generally be less detailed and less accurate.

Figure 4.19 is an approximate model obtained by defining the gross features of the true model and smoothing the slowness within each of the defining regions. This is the same model used by Nichols and it is intended to to be a realistic representation of what an explorationist might reasonably attain using geological information, velocity estimation, and well information.

Figure 4.20 is the result of standard Kirchhoff migration with first-arrival traveltimes calculated from the surface using the approximate velocity model. There is not too much difference between this and the same migration using the actual velocity model (Figure 4.7). The result of layer-stripping Kirchhoff migration is presented in Figure 4.21. The anticline and target structure is imaged, but not as well as with the actual velocity model (Figure 4.13).

Figure 4.22 is a comparison of the target zone images generated with the approximate velocity and the actual velocity. Although the image obtained with the exact velocity is superior, the one obtained with the approximate velocity is surprisingly good. All the relevant features of the target are imaged, even though the lateral coherency and structural definition are not as good as when the actual velocity is used. This shows that although the method is sensitive to velocity, it still produces a good image which could be improved by a refinement of the velocity model.

4.6 Implications for velocity estimation and 3-D imaging

Breaking up the velocity model into more manageable portions has favorable implications for both velocity estimation and 3-D applications. I will discuss some of these advantages below.

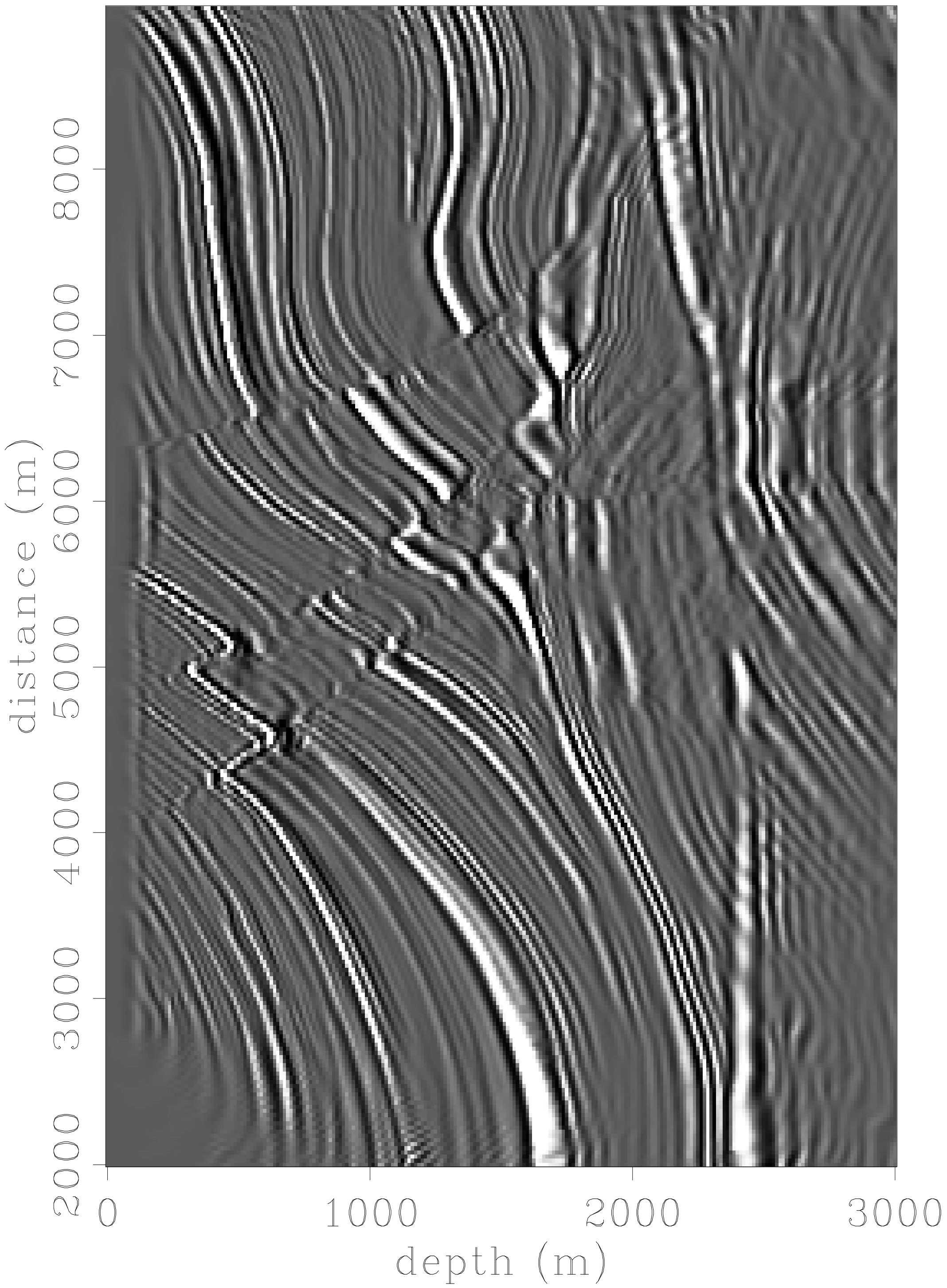

FIG. 4.15. Finite-difference shot-profile migration. Movie. Layer-shot-prof [CR]

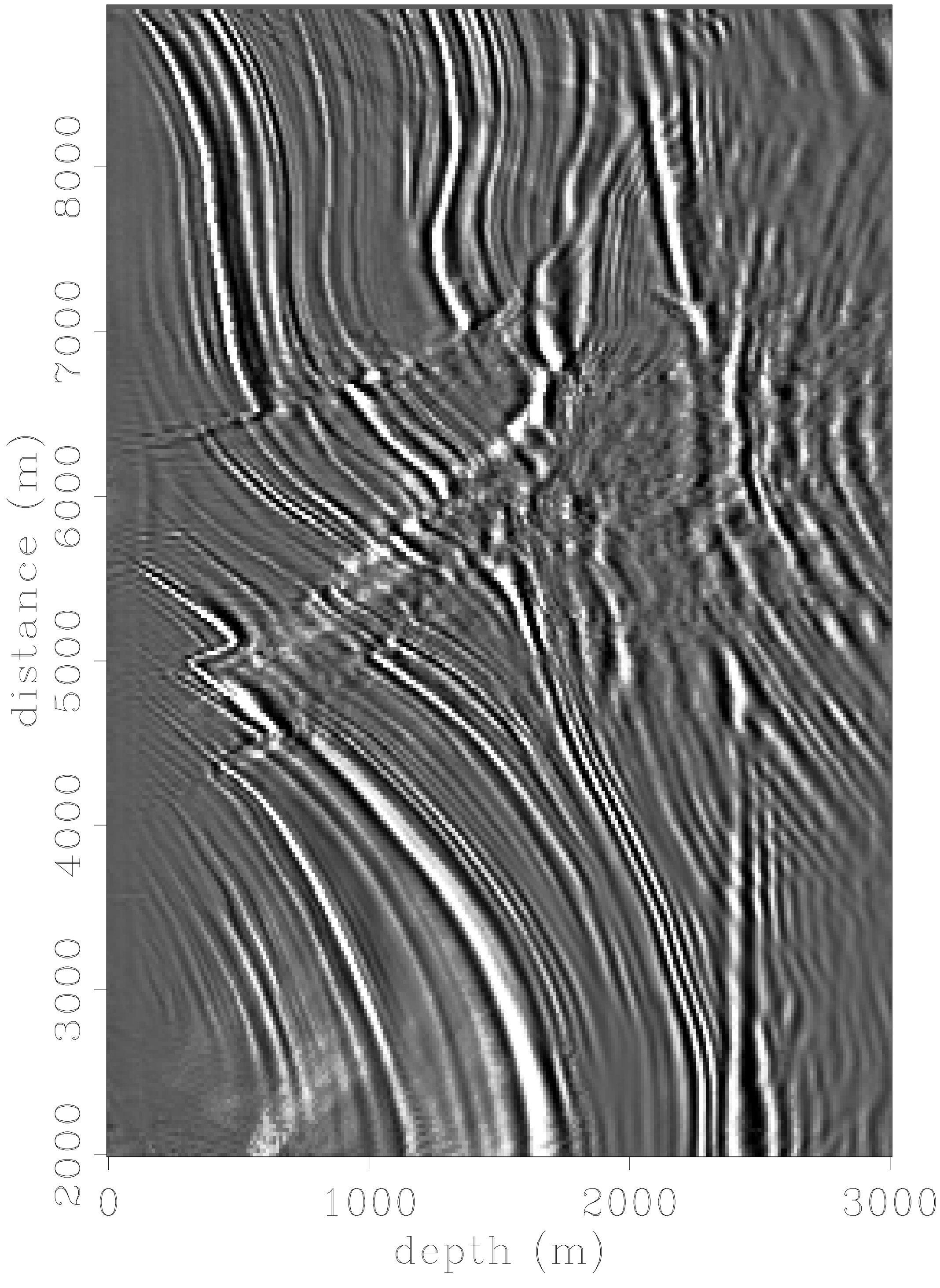

FIG. 4.16. Kirchhoff migration with paraxial traveltimes. Compare to Figure 4.13. Movie.
Layer-paraxial [CR]

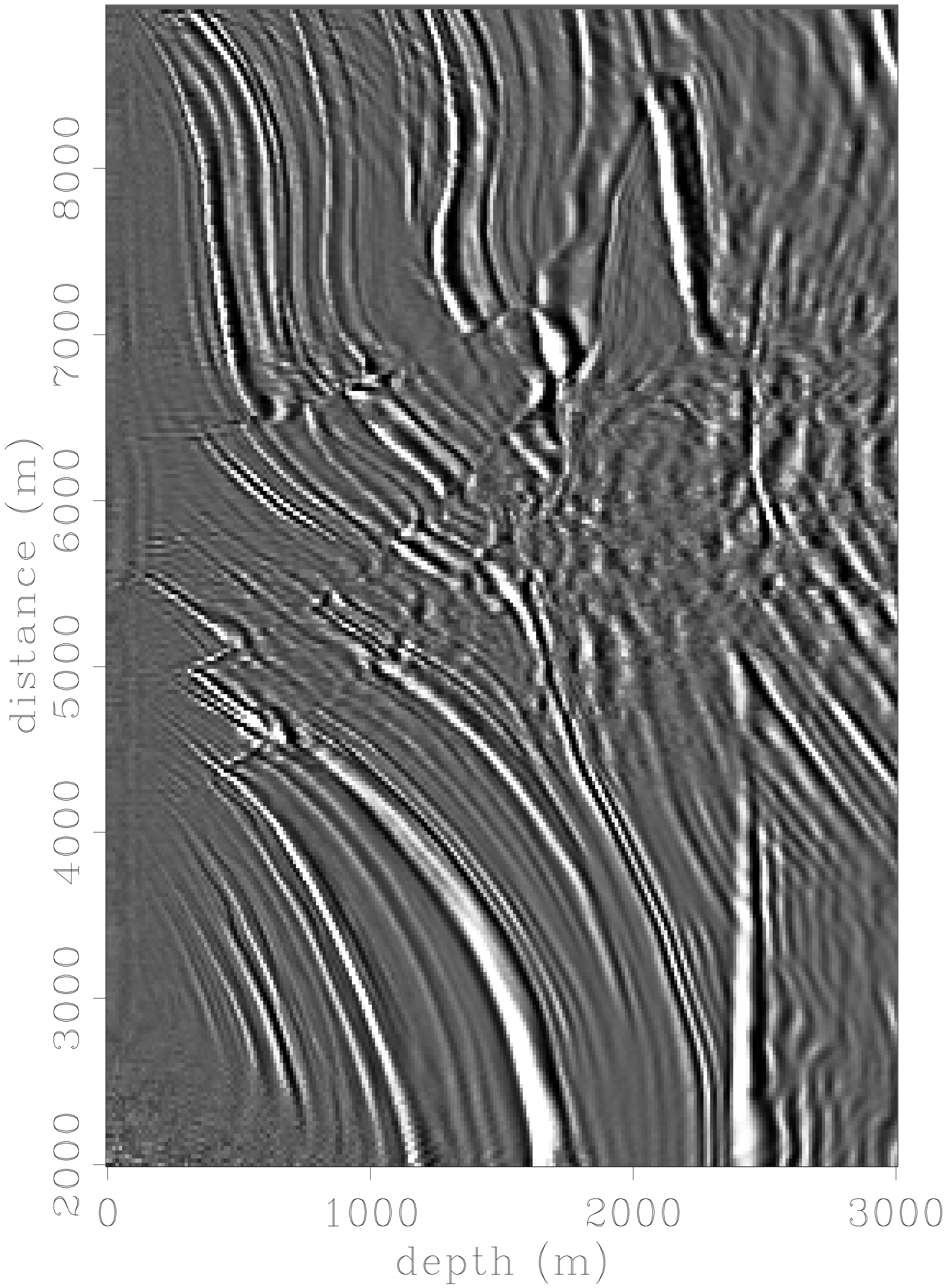

FIG. 4.17. Kirchhoff migration with band-limited traveltimes. Compare to Figure 4.13. Movie. Layer-bandlim [CR]

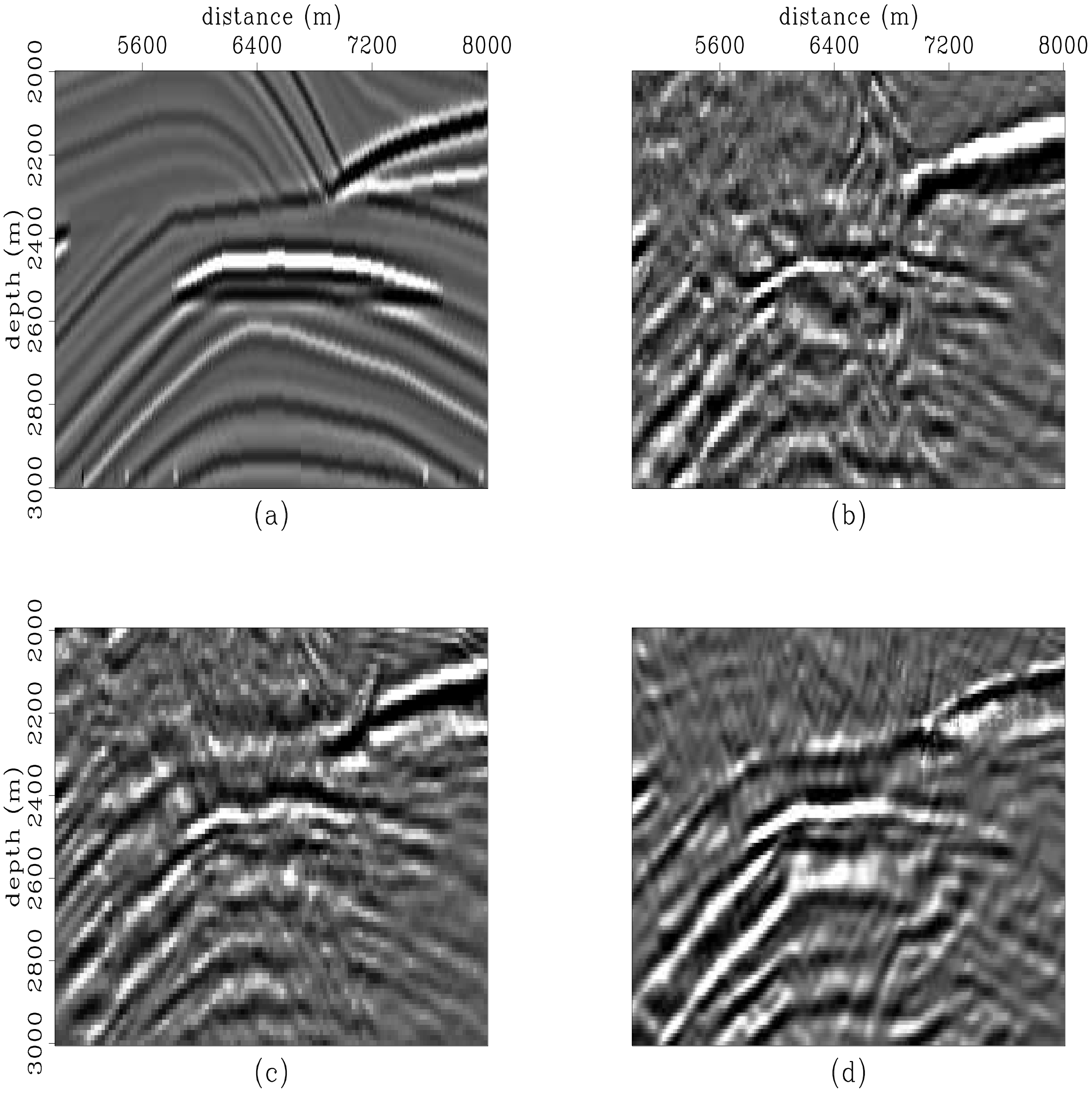

FIG. 4.18. Closeup comparison at the target zone of (a) the ideal reflectivity, images generated by (b) band-limited Kirchhoff migration, (c) paraxial traveltime Kirchhoff migration, and (d) layer-stripping Kirchhoff migration. Movie. Layer-targother [CR]

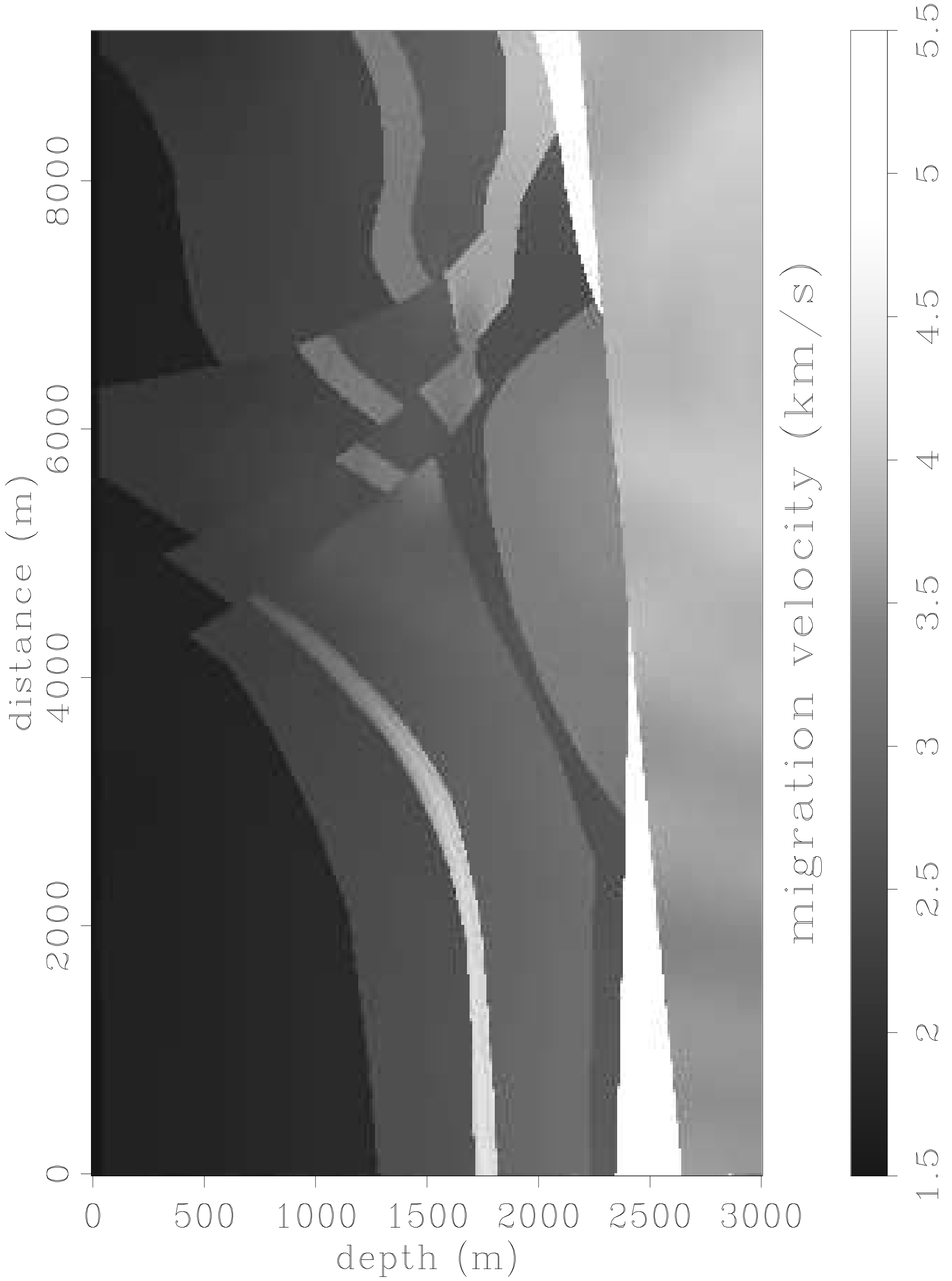

FIG. 4.19. An approximate Marmousi velocity model. Movie. Layer-velgeol [R]

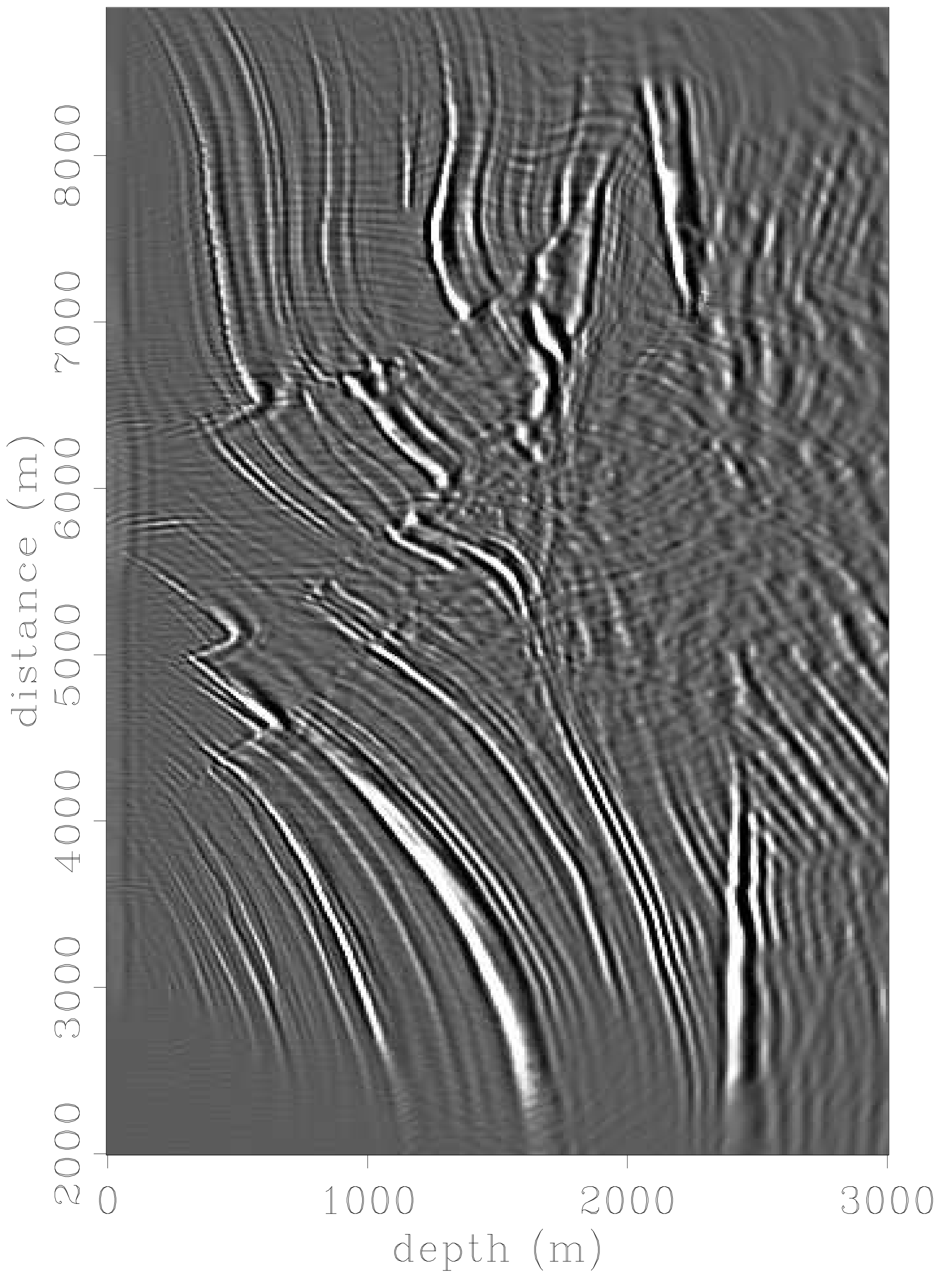

FIG. 4.20. Standard Kirchhoff migration with first-arrival traveltimes calculated from the surface using the approximate velocity model of Figure 4.19. Compare to Figure 4.7. Movie. Layer-geoleikmig [CR]

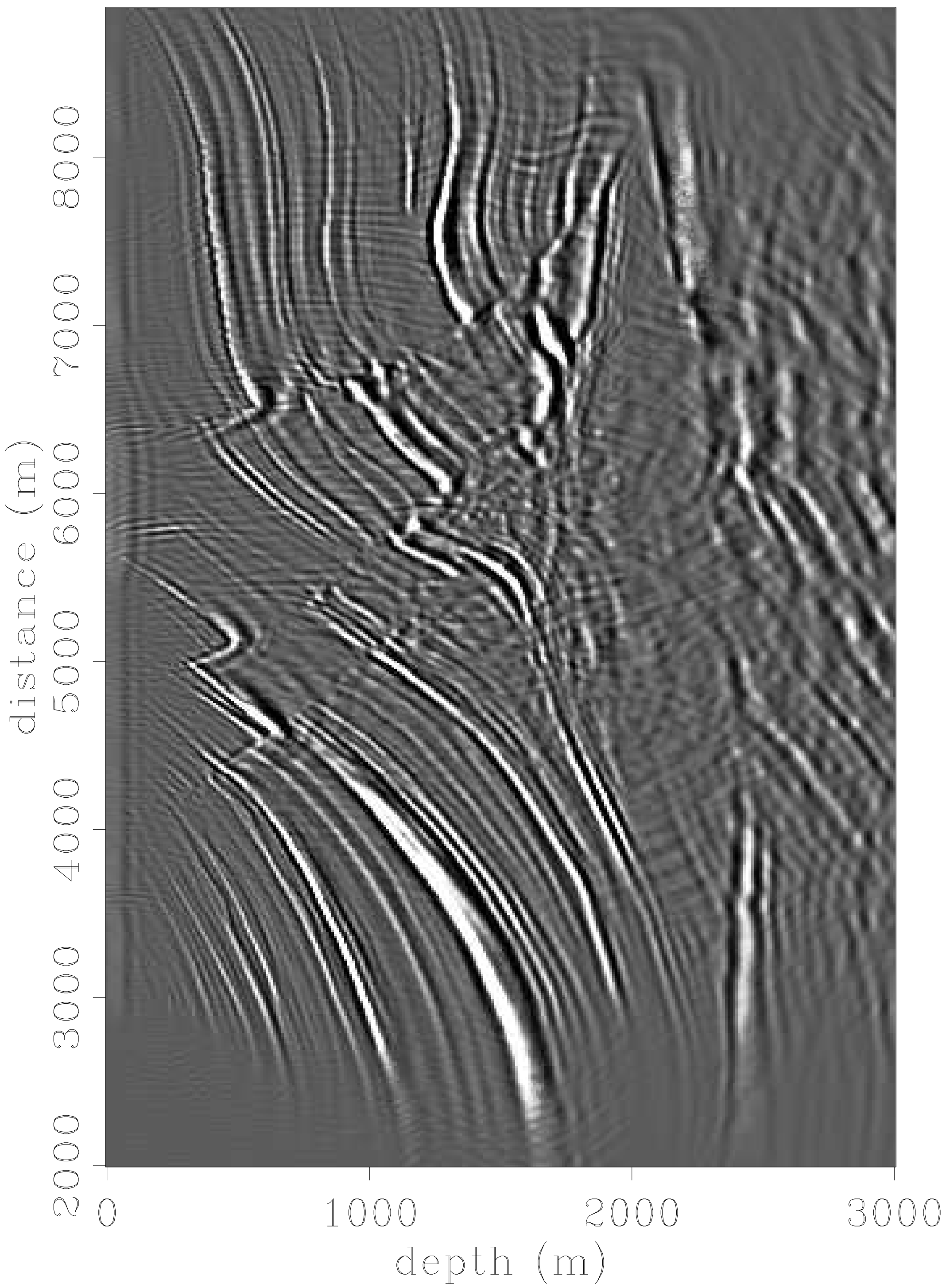

FIG. 4.21. Layer-stripping Kirchhoff migration using traveltimes calculated from the surface and traveltimes calculated from a depth of 1500 m using the approximate velocity model of Figure 4.19. The lower part of the image was obtained by migrating data which was redatumed to a depth of 1500 m in three steps of 500 m each. Compare to Figure 4.13. Movie. Layer-geolstrip3 [CR]

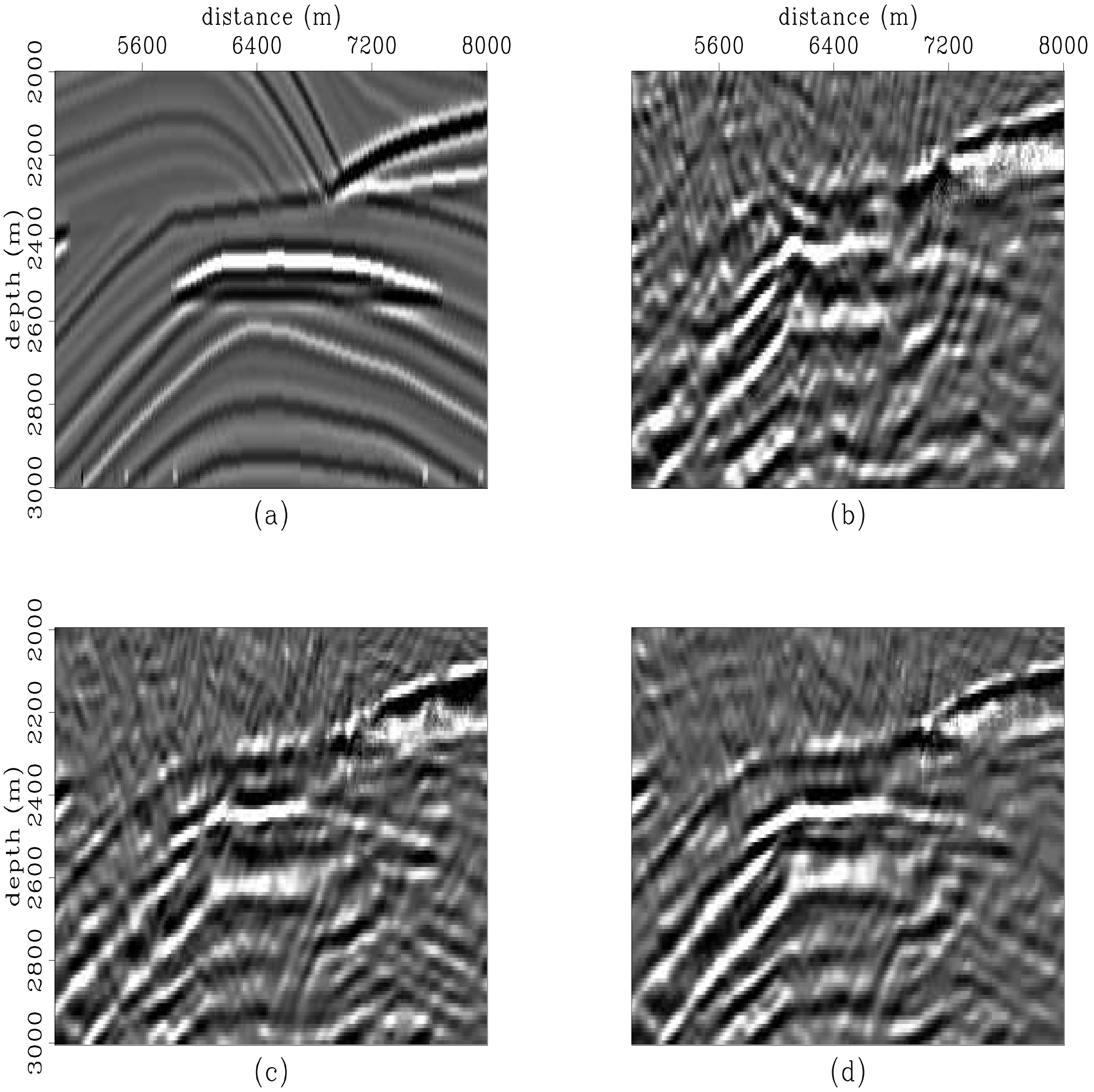

FIG. 4.22. Closeup comparison at the target zone of (a) the ideal reflectivity, (b) the image after downward continuation to 1500 m in three steps of 500 m each using the approximate velocity of Figure 4.19, (c) the image after downward continuation to 1500 m in one step with the true velocity of Figure 4.1, and (d) the image after downward continuation to 1500 m in three steps of 500 m each with the true velocity of Figure 4.1. Movie. Layer-targcomp [CR]

4.6.1 Velocity estimation

Velocity can be estimated in isolated parts of the model. By resynthesizing the data at a lower datum, I remove the complicating effects of the overlying velocity structure. For instance, the imaging problem in the lower part of the section may be simpler since compaction tends to result in velocities that are generally better behaved at depth. This means that a simpler imaging algorithm can be used at depth once the complicated overburden has been datumed through. Care should be taken to make sure that the velocity of the overlying layers is accurately determined because any error in the datuming velocity will affect the resynthesized gathers.

Even if the overlying velocity structure is not very complicated, it can be advantageous to strip it off, and perform velocity estimation and imaging from a datum that is closer to the target or the more complicated structure of interest.

A related issue is imaging and velocity estimation under anisotropic media. By means of anisotropic traveltimes, it is possible to downward continue through anisotropic layers and remove their deleterious effects. This could be very useful because in some parts of the world, there are thick anisotropic layers overlying isotropic but complex structures. The stripping off of the anisotropic layers could allow proper velocity estimation and depth imaging of the deeper portions of the data.

4.6.2 Applications to 3-D imaging

Since the layer-stripping algorithm is a Kirchhoff method, it is readily applicable to 3-D data sets. The most efficient mode of application will depend on the particular acquisition parameters and there will be intermediate data volumes. Many of the same sampling and coverage issues that arise in 3-D migration will be issues in 3-D datuming also. Depending on the acquisition geometry, the intermediate volume could turn out to be larger than the original volume because out-of-plane propagation must be accommodated and saved at intermediate depth levels.

In some cases, a common azimuth approach can be applied. This is easy to do with the Kirchhoff formulation, because it only amounts to 3-D downward continuation in what could be termed a target-oriented manner. If the cross-line lateral velocity variation is not too severe, marine data can be downward continued to a grid with the same geometry as the original acquisition geometry. In this case, some energy will be lost, but this may be acceptable.

As in the case of rugged topography, the handling of land data acquired by shooting into patches of receivers is fairly straightforward: source and receiver gathers can be extrapolated using reciprocity. In this case, source spacing will be a critical parameter in determining if the common receiver gathers will be adequately sampled.

There are several factors that can make this approach very attractive in three dimensions. All of these computational factors hold for 2-D data also, but their effects should be more dramatic in 3-D applications. The following items could offer significant efficiency in three dimensions:

- Traveltimes for 3-D imaging are usually calculated in spherical coordinates. For a given cube of desired traveltimes, this calculation requires a spherical volume with a radius equal to the longest cube diagonal. Therefore, if the velocity model is subdivided, the number of traveltimes that need to be calculated is dramatically reduced. The reduced volume also significantly reduces the storage space required during the calculation.

- After each depth step, the resynthesized data traces get progressively shorter. This means that the computation and the amount of storage per trace is reduced after each depth step.

- After each depth step, both the migration and datuming aperture can be reduced. This not only cuts down on the number of calculations, but it can be used to limit the amount of input data kept in memory for any given output location.

- As mentioned in Chapter 2, a key algorithmic difference between migration and wave-equation datuming is that each input trace is statically shifted rather than dynamically. This means that the computation can be done quickly and efficiently as a complex multiplication in the Fourier-domain, where the derivative operator is applied. This is the primary reason why an optimized Kirchhoff datuming algorithm is potentially much faster than Kirchhoff migration.

The layer-stripping migration algorithm has great potential for efficiency, and for some geometries it is more efficient than standard Kirchhoff migration.

4.7 Summary

I obtain images comparable to shot-profile migration results by combining wave-equation datuming and Kirchhoff migration into a layer-stripping migration method. In this case, first-arrival traveltimes produce satisfactory images because the velocity model is subdivided and traveltimes are calculated under conditions where finite-differencing the eikonal equation is valid. By dividing the imaging problem in this way, the traveltimes are better behaved and some multiple arrivals are accounted for.

In the example presented here, I downward continued the data to flat surfaces within the velocity model. This is not a limitation imposed by the method, and there is no reason that the data could not be downward continued to a datum which corresponds to some arbitrarily-shaped surface. For certain complex velocity models this could be an advantage because the careful choice of a surface can eliminate some potentially adverse propagation effects in the traveltime calculation.

The layer-stripping approach presented in this chapter is not limited to datuming and migration with finite-difference first-arrival traveltimes alone. The traveltime or parametric Green's function calculation can be done by any method, such as energetic ray tracing or band-limited traveltimes. The better the traveltime calculation method, the better the final image. However, in most cases, the advantage of the layer-stripping method is that computationally intensive traveltime methods need not be used.

Bibliography

Audebert, F., Biondi, B., Lumley, D., Nichols, D., Rekdal, T., and Urdaneta, H., 1994b, Marmousi Traveltime Computation and Imaging Comparisons, Stanford Expl. Proj. Report **80**, 47–66

Beasley, C., and Lynn, W., 1992, The zero-velocity layer: Migration from irregular surfaces: Geophysics, **57**, 1435–1443.

Berkhout, A. J., 1982, Seismic migration: Imaging of acoustic energy by wave field extrapolation: Elsevier, Amsterdam

Berryhill, J. R., 1979, Wave equation datuming: Geophysics, **44**, 1329–1344.

Berryhill, J. R., 1984, Wave equation datuming before stack (short note): Geophysics, **49**, 2064–2067.

Berryhill, J. R., 1986, Submarine canyons - velocity replacement by wave equation datuming before stack: Geophysics, **51**, 1572–1579.

Bevc, D., 1991, Refraction statics in mountainous terrain: Stanford Expl. Proj. Report **72**, 177–180.

Bevc, D., 1993, Data-parallel wave equation datuming with irregular acquisition topography: 63nd Ann. Internat. Mtg., Soc. Expl. Geophys., Expanded Abstracts, 197–200.

Barut, M., de Bazelaire, E., Ravat, J., and Taveau, G., A methodology to image tectonically complex areas using Polystack and prestack depth migration, *in* Versteeg, R., and Grau, G., Eds., The Marmousi experience, Proceedings of the 1990 EAEG workshop on Practical Aspects of Seismic Data Inversion: Eur. Assoc. Expl. Geophys., 159–167.

Bourgeois A., Bourget M., Lailly P., Poulet M., Ricarte P., Versteeg R., 1991, Marmousi, model and data, *in* Versteeg, R., and Grau, G., Eds., The Marmousi experience, Proceedings of the 1990 EAEG workshop on Practical Aspects of Seismic Data Inversion: Eur. Assoc. Expl. Geophys., 5–16.

Burke, N. L., and Knapp, S., 1995, Imaging advances in the Columbian foothills: The Leading Edge, **14**, 677–679.

Biondi, B., 1992, Solving the frequency-dependent eikonal equation: 62nd Ann. I nternat. Mtg., Soc. Expl. Geophys., Expanded Abstracts, 1315–1319.

Claerbout, J. F., 1985, Imaging the Earth's Interior: Blackwell Scientific Publications.

Gazdag, J., 1978, Wave equation migration with the phase shift method: Geophysics, **43**, 1342–1351.

Gazdag, J., and Sguazzero, P., 1984, Migration of seismic data by phase shift plus interpolation: Geophysics, **49**, 124–131.

Geoltrain, S. and Brac, J., 1993, Can we image complex structure with first-arrival traveltime?, Geophysics **58**, 564–575

Gray, S. H., and May, W. P., 1993, Kirchhoff migration using eikonal equation traveltimes, Geophysics **59**, 810–817

Ji, J., and Claerbout, J. F., 1992, Phase shift datuming and migration from an irregular surface: Stanford Expl. Proj. Report **75**, 157-170.

Karrenbach, M., 1995, Elastic tensor wave fields: Ph.D. Thesis, Stanford University.

Lomax, A. J., 1992, An approximate method of modeling broadband wave propagation through complex, inhomogenous media: Ph.D. Thesis, University of California, Berkeley.

Nichols, D., 1994, Imaging complex structures using band limited Green's functions, Ph.D. Thesis, Stanford University.

Popovici, A. M., 1991, Finite-difference traveltime maps: Stanford Expl. Proj. Report **70**, 245–256.

Popovici, A. M., 1992, Wave-equation datuming in variable velocity media: Stanford Expl. Proj. Report **75**, 191–214.

Reshef, M., 1991, Depth migration from irregular surfaces with depth extrapolation methods (short note): Geophysics, **56**, 119–122.

Shtivelman, V., and Canning, A., 1988, Datum correction by wave equation extrapolation: Geophysics, **53**, 1311-1322.

Schneider, W. A. Jr., Phillip, L. D., Paal, E. F., 1995, Wave-equation velocity replacement of the low-velocity layer for overthrust-belt data: Geophysics, **60**, 573–580.

Schneider, W. A., 1978, Integral Formulation for Migration in Two-Dimensions and Three-Dimensions: Geophysics, **43**, 49–76.

Tilander, N. G., and Mitchel, R. G., 1995 Processing seismic data from overthrust areas in Latin America: The Leading Edge, **14**, 707–713.

van Trier, J., and Symes, W. W., 1991, Upwind finite-difference calculation of traveltimes: Geophysics, **56**, 812–821.

Wiggins, J. W., 1984, Kirchhoff integral extrapolation and migration of nonplanar data: Geophysics, **49**, 1239–1248.

Yilmaz, O., and Claerbout, J. F., 1980, Prestack partial migration: Geophysics, **45**, 1753–1779

Yilmaz, O., and Lucas, D., 1986, Prestack layer replacement: Geophysics, **51**, 1355–1369.